






Stable-fixed-point description of square-pattern formation in driven two-dimensional Bose-Einstein condensates

Keisuke Fujii ^{1,*} Sarah L. Görlitz,¹ Nikolas Liebster,^{2,†} Marius Sparn,² Elinor Kath ² Helmut Strobel,² Markus K. Oberthaler ² and Tilman Enss ¹

¹*Institut für Theoretische Physik, Universität Heidelberg, Philosophenweg 19, 69120 Heidelberg, Germany*

²*Kirchhoff-Institute für Physik, Universität Heidelberg, Im Neuenheimer Feld 227, 69120 Heidelberg, Germany*

 (Received 20 September 2023; revised 23 April 2024; accepted 23 April 2024; published 10 May 2024)

We investigate pattern formation in two-dimensional Bose-Einstein condensates (BECs) caused by periodic driving of the interatomic interaction. We show that this modulation generically leads to a stable square grid density pattern, due to nonlinear effects beyond the initial Faraday instability. We take the amplitudes of two waves parametrizing the two-dimensional density pattern as order parameters in pattern formation. For these amplitudes, we derive a set of coupled time-evolution equations from the Gross-Pitaevskii equation with a time-periodic interaction. We identify the fixed points of the time evolution and show by stability analysis that the inhomogeneous density exhibits a square grid pattern, which can be understood as a manifestation of a stable fixed point. Our stability analysis establishes the pattern in BECs as a nonequilibrium steady state.

DOI: [10.1103/PhysRevA.109.L051301](https://doi.org/10.1103/PhysRevA.109.L051301)

Introduction. In recent years, there has been intense interest in many-body dynamics far from equilibrium. Among these dynamics, pattern formation is particularly intriguing, as uniform states spontaneously become inhomogeneous when external parameters change. As a spontaneous breaking of symmetry in dynamics, pattern formation appears in nature at diverse scales, not only in physics [1,2] but also in chemical reactions [3] and biology [4]. However, important questions remain unanswered due to the need for highly controlled experiments. Thus, ultracold atomic systems are well suited to study pattern formation, due to their advanced experimental techniques.

In Bose-Einstein condensates (BECs), spontaneous pattern formation arises from temporal modulations of system parameters, such as the magnitudes of trapping potentials and interactions [5]. This parametric instability is also known as the Faraday instability, as an analogy to a similar phenomenon in classical fluids [6–10]. Indeed, observations in BECs include one-dimensional patterns [11–13] and surface patterns of a two-dimensional system [14]. Furthermore, in two-dimensional systems, the symmetry of selected patterns can be engineered through multiple simultaneous modulations of the atomic interactions [15]. Theoretically, parametric instabilities derived from linear analysis in driven one-dimensional quantum gases have been actively studied, and many studies have calculated the wave number of excitations generated by the instability [16–47].

However, previous studies have neglected the effects of nonlinearities and their role in stabilizing certain geometries of patterns far beyond the linear regime. This is particularly

relevant in two dimensions, where structures are characterized by both lattice symmetry and wave number. In our recent companion work [48], we observed two-dimensional stable patterns, clearly exhibiting a square grid, with a single-frequency modulation of the interaction without fine-tuning. In particular, this emergence of square grids contrasts with previous theoretical claims of an oblique grid realization in Ref. [5], underlining the importance of a theoretical investigation of the underlying mechanisms.

In this Letter, we introduce an analytical method that describes not only the growth but also the stabilization of certain patterns due to nonlinearities in driven single-component BECs. We derive time-evolution equations for the amplitudes of density waves spanning two-dimensional patterns in BECs. We show that driven condensates exhibit a square grid as a stable pattern. In our model, we consider density modulations in two directions \mathbf{k} and \mathbf{p} in the plane with amplitudes R_k and R_p , respectively. When the angle between the two directions is near $\pi/2$, both amplitudes grow to finite values and we find that the system exhibits a stable grid pattern. Conversely, for small angles, only one of the amplitudes grows to a finite value while the other is suppressed, and the BEC exhibits a stripe pattern. This result is clearly seen in Fig. 1, where the global stability of the patterns differs significantly depending on the angle between the two directions. In the experiment, many modes at different angles initially grow due to the instability, and our analysis shows that two of these modes at an angle close to $\pi/2$ will reinforce each other and grow into a grid pattern, while other modes at small angles are suppressed.

BEC with a time-periodically-modulated interaction. We consider a two-dimensional BEC with an interaction strength $g(t) = \bar{g}[1 - A \sin(\omega t)]$ with drive amplitude $|A| < 1$ around its mean value \bar{g} . The dynamics of a BEC with wave function $\Psi(t, \mathbf{x})$ is described by the Gross-Pitaevskii (GP)

*fujii@thphys.uni-heidelberg.de

†pattern-formation@matterwave.de

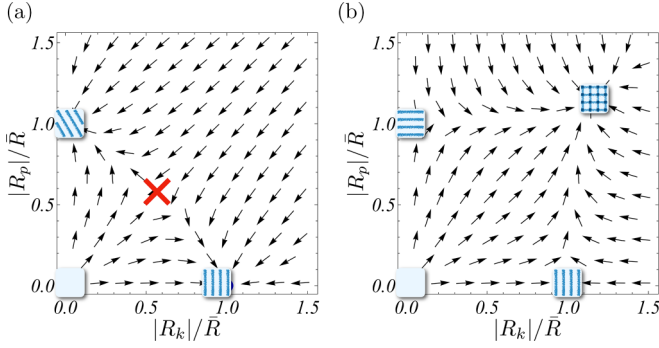


FIG. 1. Global stability of the patterns formed by two standing waves in a planar BEC in directions \mathbf{k} and \mathbf{p} . Schematic figures at the fixed points represent corresponding stationary solutions, i.e., the grid-pattern, stripe-pattern, and uniform solutions. The angle θ between the two excited modes is (a) $\theta = \angle(\mathbf{k}, \mathbf{p}) = \pi/6$ and (b) $\theta = \angle(\mathbf{k}, \mathbf{p}) = \pi/2$. In the latter case, the square grid pattern emerges as a stable fixed point. The parameters are $\omega/\mu = 2$ and $A = 0.6$ with low dissipation $\Gamma = 0.1\alpha$, where ω , μ , and α are the driving frequency, the chemical potential, and the drive amplitude, respectively.

equation [49]

$$i \frac{\partial}{\partial t} \Psi(t, \mathbf{x}) = \left(-\frac{\nabla^2}{2m} + g(t) |\Psi(t, \mathbf{x})|^2 \right) \Psi(t, \mathbf{x}), \quad (1)$$

where we set $\hbar = 1$. We assume an infinitely extended BEC without trapping potential term.

Equation (1) has a uniform solution $\Psi_{\text{uni}}(t) = \Psi_0 \exp[-i\mu t - i(\mu/\omega)A \cos(\omega t)]$ with the chemical potential $\mu = \bar{g}|\Psi_0|^2$, but this solution becomes unstable due to the Faraday instability induced by the oscillating interaction [5]. This instability can be understood to be caused by a selective amplification of excited modes with wave vector \mathbf{k} satisfying the resonance condition $n\omega/2 = E_k$ for $n \in \mathbb{N}$. Here $E_k = \sqrt{\epsilon_k(\epsilon_k + 2\mu)}$ and $\epsilon_k = \mathbf{k}^2/2m$ represent the Bogoliubov quasiparticle and single-particle dispersions, respectively. The resonance condition $n\omega/2 = E_k$ comes from the fact that the energy quantum $n\omega$, injected into the system by the oscillation, excites two Bogoliubov modes characterized by wave vectors \mathbf{k} and $-\mathbf{k}$. Within a linear stability analysis, one can indeed derive Mathieu's differential equation from Eq. (1), which shows the amplification of modes with wave numbers around the resonance condition [50].

Amplitude equation. Beyond this linear instability analysis, large occupations and nonzero background interactions can lead to competition between the exponential growth and nonlinear suppression of growth. Additionally, in two dimensions, nonparallel density waves are coupled due to this nonlinearity, leading to stable grid patterns. We determine the magnitude of the amplitude and the angle of the realized grid, assuming that the drive amplitude A is small. In this case, the amplitude of the density pattern grows slowly and its time evolution is systematically obtained as slow-timescale dynamics. Using the multiple-scale method [1,2], we derive the time-evolution equation for the pattern amplitude from Eq. (1).

We expand the wave function as [51]

$$\Psi(t, \mathbf{x}) = \Psi_{\text{uni}}(t) [1 + \phi_k(t) \cos(\mathbf{k} \cdot \mathbf{x}) + \phi_p(t) \cos(\mathbf{p} \cdot \mathbf{x})]. \quad (2)$$

At small drive amplitude A , the excitation $\phi_{k,p}$ is naturally expressed in the Bogoliubov basis

$$\begin{aligned} \phi_{k,p}(t) = & \left(1 - \frac{\epsilon_{k,p} + 2\mu}{E_{k,p}} \right) R_{k,p}(t) e^{i\omega t/2} \\ & + \left(1 + \frac{\epsilon_{k,p} + 2\mu}{E_{k,p}} \right) R_{k,p}^*(t) e^{-i\omega t/2}, \end{aligned} \quad (3)$$

where the complex amplitudes $R_{k,p}(t)$ obey a complex Ginzburg-Landau-type equation (for the detailed derivation, see the Supplemental Material [52])

$$\begin{aligned} i \frac{d}{dt} R_k(t) = & \Delta R_k(t) - i\alpha R_k^*(t) + \lambda [|R_k(t)|^2 R_k(t) \\ & + c_1(\theta) |R_p(t)|^2 R_k(t) + c_2(\theta) R_p(t)^2 R_k^*(t)], \end{aligned} \quad (4)$$

with detuning $\Delta = \omega/2 - E_k$, drive amplitude for the Bogoliubov mode $\alpha = \mu A \epsilon_k / 2E_k$, and nonlinearity $\lambda = \mu(5\epsilon_k + 3\mu)/E_k$. The same equation holds for $R_p(t)$ after exchange of the \mathbf{k} and \mathbf{p} labels. In order to focus on the angle of the realized pattern, we assume that the absolute values of the wave vectors \mathbf{k} and \mathbf{p} are equal, as determined by the resonance condition $\Delta = 0$ for $n = 1$, and set $\epsilon_k = \epsilon_p = \epsilon$ and $E_k = E_p = E$. The coupling coefficients $c_1(\theta)$ and $c_2(\theta)$ between modes in different directions are then given as functions of the angle $\theta \in [0, \pi/2]$ between \mathbf{k} and \mathbf{p} ,

$$\begin{aligned} c_1(\theta) = & \frac{\mu}{5\epsilon + 3\mu} \left[4 \frac{\epsilon^2 - \mu^2}{\mu\epsilon} + \left(\frac{2\epsilon + \mu}{\epsilon} \frac{2\epsilon + \mu}{\epsilon_+ / 2 + \mu} \right. \right. \\ & \left. \left. - \frac{(2\epsilon - \mu)(\epsilon + 2\mu) + (2\epsilon^2 + \mu^2)\epsilon_+ / 2\epsilon}{E^2 - E_+^2 / 4} \right. \right. \\ & \left. \left. + (\epsilon_+ \rightarrow \epsilon_-) \right) \right], \end{aligned} \quad (5a)$$

$$\begin{aligned} c_2(\theta) = & \frac{\mu}{5\epsilon + 3\mu} \left[-2 \frac{\epsilon^2 + 3\mu\epsilon + \mu^2}{\mu\epsilon} \right. \\ & \left. + \frac{2\epsilon + \mu}{\epsilon} \left(\frac{2\epsilon + \mu}{\epsilon_+ / 2 + \mu} + (\epsilon_+ \rightarrow \epsilon_-) \right) \right], \end{aligned} \quad (5b)$$

where we introduced $E_{\pm} = \sqrt{\epsilon_{\pm}(\epsilon_{\pm} + 2\mu)}$ with $\epsilon_+ = \epsilon_{\mathbf{k}+\mathbf{p}} = 4\epsilon \cos^2 \frac{\theta}{2}$ and $\epsilon_- = \epsilon_{\mathbf{k}-\mathbf{p}} = 4\epsilon \sin^2 \frac{\theta}{2}$ [53].

Equation (4) is referred to as the amplitude equation. While also other pattern-forming phenomena in classical liquids are understood from amplitude equations, these equations cannot be applied to BECs because incompressibility is typically assumed for classical fluids, e.g., for the case of Faraday patterns in water [7,8]. Instead, BECs are compressible and exhibit density and phase fluctuations, which are reflected in the complex-valued nature of the amplitudes. Accordingly, our amplitude equation has a nonlinear term proportional to $c_2(\theta)$, which is absent in other amplitude equations for standing-wave patterns. This distinction highlights the differences in the pattern stabilization mechanism between BECs and classical incompressible fluids.

Fixed points and their stability analysis. The time-dependent solutions of the amplitude equation trace out trajectories in the four-dimensional space of the two complex amplitudes. In the following, we analyze their fixed points and stability. We focus only on the populated modes satisfying the resonance condition at zero detuning $\Delta = 0$ and introduce the dissipation $\Gamma > 0$ phenomenologically to capture, for instance, the suppression from interaction with other modes besides the \mathbf{k} and \mathbf{p} modes:

$$i \frac{d}{dt} R_k(t) = -i\Gamma R_k(t) - i\alpha R_k^*(t) + \lambda[|R_k(t)|^2 R_k(t) + c_1(\theta)|R_p(t)|^2 R_k(t) + c_2(\theta)R_p(t)^2 R_k^*(t)]. \quad (6)$$

The dissipation term effectively captures dynamics beyond the two modes of interest, leading to irreversible evolution of the reduced system, even though the underlying GP equation is reversible [54]. Setting $dR_k(t)/dt = 0$ in Eq. (6) and similarly for $R_p(t)$, we find four possible fixed-point values of R_k and R_p ,

$$R_k = R_p = 0 \quad (\text{fixed point } U), \quad (7a)$$

$$R_k = \bar{R}e^{i\bar{\eta}}, \quad R_p = 0 \quad (\text{fixed point } S_k), \quad (7b)$$

$$R_k = 0, \quad R_p = \bar{R}e^{i\bar{\eta}} \quad (\text{fixed point } S_p), \quad (7c)$$

$$R_k = R_p = \bar{R}e^{i\bar{\eta}}/\sqrt{1 + c_1(\theta) + c_2(\theta)} \quad (\text{fixed point } G), \quad (7d)$$

with $\bar{R}^2 = \sqrt{\alpha^2 - \Gamma^2}/\lambda$ and $\exp(i\bar{\eta}) = (\sqrt{\alpha - \Gamma} + i\sqrt{\alpha + \Gamma})/\sqrt{2\alpha}$. The fixed points correspond to the following density patterns: U , a uniform pattern; S_k and S_p , stripe patterns for each direction; and G , a grid pattern (see Fig. 1).

We first investigate the stability of the uniform fixed point U . For small $R_k(t)$ and $R_p(t)$ around U , only the linear terms of Eq. (6) remain, and the \mathbf{k} and \mathbf{p} directions become independent. By dividing the linearized equation into its real and imaginary parts, we directly find the eigenvalues of the Jacobian (scaling dimensions) as $\Lambda = -\Gamma - \alpha, -\Gamma + \alpha$. Since the amplitudes scale as $e^{\Lambda t}$ around the fixed point (unstable for $\text{Re } \Lambda > 0$, stable for $\text{Re } \Lambda < 0$, and center for $\text{Re } \Lambda = 0$), the fixed point U is unstable for $\alpha > \Gamma$. This corresponds to the Faraday instability, in which the uniform solution becomes unstable when the drive is stronger than the dissipation.

We next study the stability of the grid fixed point G . The four eigenvalues of the amplitude equation linearized around G are found to be

$$\Lambda_1^\pm = -\Gamma \pm i\sqrt{4\alpha^2 - 5\Gamma^2}, \quad (8a)$$

$$\Lambda_2^\pm = -\Gamma \pm \frac{\sqrt{4(\alpha^2 - \Gamma^2)D(\theta) + \Gamma^2(1 + c_1 + c_2)^2}}{1 + c_1 + c_2}, \quad (8b)$$

with $D(\theta) \equiv -1 + c_1(\theta)^2 + 2c_2(\theta) - c_2(\theta)^2$. While the real part of the first eigenvalue Λ_1^\pm is negative for $\alpha > \Gamma$, the second eigenvalue Λ_2 has a negative real part only when

$$D(\theta) < 0. \quad (9)$$

The inequality (9) thus provides the condition for the grid pattern to be stable, regardless of the magnitude of the dissipation Γ . Note that the stability analysis around the fixed points S_k

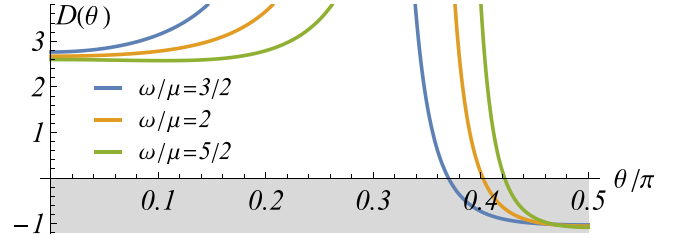


FIG. 2. Stability criterion for the grid pattern: $D(\theta)$ as a function of $\theta = \angle(\mathbf{k}, \mathbf{p}) \in [0, \pi/2]$ with fixed $A = 0.6$ for different values of ω/μ . The grid pattern for angles $\theta \approx \pi/2$ is stable where $D(\theta) < 0$ (gray-shaded region).

and S_p leads to the inverse inequality $D(\theta) > 0$, indicating that stripes are stable when grids are unstable and vice versa. As seen in Fig. 2, the grid pattern is stable around an angle of $\theta = \pi/2$, which is consistent with the experimental results [48]. Note that the coefficient $c_2(\theta)$ is negative around $\theta = \pi/2$ and therefore enhances the stability of the square pattern.

In the absence of dissipation, the eigenvalues always appear in positive and negative pairs, such as Eq. (8) with $\Gamma = 0$, because the amplitude equation without dissipation fulfills the time-reversal symmetry inherited from the GP equation. The behavior of the solution in the four-dimensional space near the fixed points can be understood separately for each two-dimensional subspace corresponding to each pair of positive and negative eigenvalues. Without dissipation, the pair of eigenvalues with a real part makes the fixed point in the corresponding two-dimensional subspace a saddle point, while the pure imaginary pair makes the fixed point a center. A small dissipation $\Gamma < \alpha$ keeps the saddle fixed point as a saddle while turning the center into a stable focus (in-spiral).

Let us investigate the global behavior of the solutions of the amplitude equation beyond the local behavior around the fixed points. When we introduce the real and imaginary parts of the phase-rotated amplitudes as $\rho_{k,p} = \text{Re}(R_{k,p}e^{-i\bar{\eta}})$ and $v_{k,p} = \text{Im}(R_{k,p}e^{-i\bar{\eta}})$, all four fixed points lie in the two-dimensional subspace spanned by ρ_k and ρ_p with $v_k = v_p = 0$. The four-dimensional flow trajectories still depart from an unstable fixed point (saddle) and approach an attractive one (in-spiral). This global behavior can be visualized by utilizing the square eigenvalue Λ^2 , which is positive (repulsive) for real Λ at the saddle, while it is negative (attractive) for imaginary Λ at the in-spiral. We can efficiently obtain the square eigenvalues via the second-order differential equation derived from the amplitude equation (6), which is given by

$$\begin{aligned} \left. \frac{d^2}{dt^2} \rho_k(t) \right|_{v_k=v_p=0} &= \lambda^2 [\bar{R}^2 + \rho_k(t)^2 + (c_1 - c_2)\rho_p(t)^2] \\ &\quad \times [\bar{R}^2 - \rho_k(t)^2 - (c_1 + c_2)\rho_p(t)^2] \rho_k(t) \\ &\quad + 2\lambda^2 c_2 [\bar{R}^2 - \rho_p(t)^2 - (c_1 + c_2)\rho_k(t)^2] \rho_p(t)^2 \rho_k(t) \end{aligned} \quad (10)$$

and likewise for $\rho_p(t)$ after exchanging the $\rho_k(t)$ and $\rho_p(t)$ variables. The force field described by the right-hand side of Eq. (10) captures the global behavior of the solution of the original amplitude equation. This global behavior is shown

in Fig. 1 and it changes drastically depending on the angle between \mathbf{k} and \mathbf{p} [55].

Three-mode amplitude equation. At a specific angle satisfying $2E = E_+$, two Bogoliubov modes with wave vectors \mathbf{k} and \mathbf{p} can resonantly scatter into a Bogoliubov mode with wave vector $\mathbf{k} + \mathbf{p}$ without violating energy conservation, which enhances the contribution of this collision process. Therefore, the amplitude of the wave vector $\mathbf{k} + \mathbf{p}$, which grows proportionally to both the amplitudes R_k and R_p , cannot be neglected, and its omission in the two-mode ansatz (2) causes a divergence of the coefficient $c_1(\theta)$ in Eq. (5a) at this specific angle. This same divergence is seen in Fig. 2, e.g., at $\theta \approx 0.34\pi$ for $\omega/\mu = 2$. We now present the complete theory without divergence and show that no other (e.g., triangular) patterns appear near this singular angle. By additionally including the $\mathbf{k} + \mathbf{p}$ mode described by the complex amplitude $R_+(t)$ in the ansatz (2), we derive the coupled amplitude equations for the three modes $R_{k,p}(t)$ and $R_+(t)$ as (for details of the derivation and the coefficients see [52])

$$i \frac{d}{dt} R_k(t) = -i\Gamma R_k(t) - i\alpha R_k^*(t) - \beta(\theta) R_+(t) R_p^*(t) + \lambda[|R_k(t)|^2 R_k(t) + \tilde{c}_1(\theta) |R_p(t)|^2 R_k(t) + c_2(\theta) R_p(t)^2 R_k^*(t)], \quad (11a)$$

$$i \frac{d}{dt} R_+(t) = -i\Gamma_+ R_+(t) + \Delta_+(\theta) R_+(t) - \beta_+(\theta) R_k(t) R_p(t) + \lambda_+(\theta) |R_+(t)|^2 R_+(t), \quad (11b)$$

where Γ and Γ_+ are dissipation coefficients. We find that the coefficient $\tilde{c}_1(\theta)$ has no divergence at the singular angle satisfying $2E = E_+$ and all coefficients in Eq. (11) are regular in $\theta \in [0, \pi/2]$. We note that the \mathbf{k} and \mathbf{p} modes now interact with the $\mathbf{k} + \mathbf{p}$ mode via quadratic terms in the amplitude equation (three-mode scattering).

Using Eq. (11), we can numerically simulate the time evolution for various initial conditions at a fixed angle between \mathbf{k} and \mathbf{p} . The top left part of Fig. 3 shows the simulation results of the time evolution of the amplitudes from an initial state close to a uniform pattern at $\theta = \pi/2$, demonstrating that the system arrives at a grid pattern with all amplitudes finite. Repeating these simulations for different angles θ , we arrive at the phase diagrams for the three-mode and two-mode models shown in Fig. 3. In both phase diagrams, the grid pattern is stable in a region around $\theta = \pi/2$, and the phase diagrams are in good agreement. Notably, the three-mode model (11) has no singularity in its coefficients and its phase diagram is reliable over the entire range of angles $\theta \in [0, \pi/2]$. Furthermore, using Eq. (11), we investigate the stability to changes in the grid angle θ and numerically confirm that the square grid with $\theta = \pi/2$ is the most stable among the stable grids as indicated by the arrows in the phase diagram of Fig. 3 (see the Supplemental Material [52] for a detailed discussion).

Discussion and outlook. Before concluding, we briefly discuss the scattering between the three modes satisfying $\mathbf{k}_1 \pm \mathbf{k}_2 \pm \mathbf{k}_3 = \mathbf{0}$, which usually leads to a triangular pattern [2]. In the Faraday pattern formation, the leading three-mode scattering occurs at the frequency $\omega/2 \pm \omega/2 \pm \omega/2$ because the excited modes have energy $\omega/2$ from the first resonance

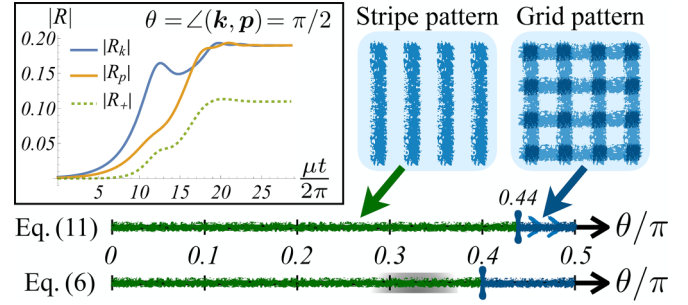


FIG. 3. Phase diagram of the stable patterns in the three-mode model (11) and the two-mode model (6) with parameters $(A, \omega/\mu, \Gamma/\alpha, \Gamma_+/\alpha) = (0.6, 2, 0.5, 1)$. While angles in the green region have stable stripe solutions, angles in the blue region have stable lattice solutions, as shown schematically in the top right corner. The phase diagram for Eq. (6) is obtained analytically from the inequality (9) and corresponds to Fig. 2. In both cases, the grid pattern is stable around $\theta = \pi/2$, whereas the stripe pattern appears at small angles. Thus, both models predict the same grid-pattern phase, although the two-mode model is incomplete around the singular angle $\theta \approx 0.34\pi$ (gray-shaded region). Arrows in the phase diagram for Eq. (11) indicate the stability to changes in the grid angle θ , with $\theta = \pi/2$ being the most stable as discussed in the Supplemental Material [52]. The top left inset shows the numerical simulation of Eq. (11) at $\theta = \pi/2$ with initial condition $(R_k, R_p, R_+) = (0.002i, 0.001i, 0.0001)$, where initial stripes after approximately 10 cycles develop into a grid pattern after approximately 16 cycles.

condition $n = 1$. Because $\omega/2 \pm \omega/2 \pm \omega/2 \neq 0$, the three-mode scattering is a fast-rotating contribution in the rotating-wave basis and can be neglected. Instead, if the third mode satisfies the second resonance condition $n = 2$ with frequency ω instead of $\omega/2$, three-mode scattering can become relevant since it has a slow-rotating contribution with $\omega/2 + \omega/2 - \omega = 0$. In fact, the amplitude equation (11) includes this three-mode scattering. However, we found that the stability of the patterns does not change significantly between Eqs. (4) and (11).

In this Letter, we have derived the amplitude equations (6) and (11) for pattern formation in two-dimensional BECs beyond the Faraday instability. The amplitude equation can be considered as a complex Ginzburg-Landau-type equation for pattern formation with the amplitudes in the two directions as order parameters, and it provides a simple description of the system dynamics. Our method to derive the amplitude equation is equivalent to the renormalization-group theory for asymptotic analysis [56–58]. Accordingly, the amplitude equation describes the order parameter dynamics as an effective model for the only two or three relevant modes remaining at long times, while in a renormalization-group sense it incorporates the multitude of irrelevant modes of the full GP simulation in the dissipation coefficient.

Using the obtained amplitude equation, we have analyzed the stability between the uniform, stripe-pattern, and grid-pattern solutions. For $\alpha > \Gamma$, where the drive amplitude is stronger than the dissipation, the uniform solution becomes unstable, resulting in an inhomogeneous density pattern. Figures 2 and 3 show that the grid pattern becomes stable around the angle $\pi/2$ between the two excitation directions.

The global stability of the amplitude is shown in Fig. 1. In particular, in the three-mode model, taking into account the resonant scattering that occurs around the singular angles, we have shown that the grid is stable at $\pi/2$ and not at the singular angle previously suggested. Our results provide the theoretical framework for the experimental data presented in our companion paper [48]. Furthermore, the amplitude equation has been experimentally validated under various initial conditions and has been confirmed to give a good description. Our stability analysis has established patterns in superfluids as nonequilibrium steady states. Moreover, these patterns fit the definition of supersolidity as a self-stabilized superfluid state with spontaneous translational symmetry breaking, suggesting the emergence of a new type of supersolidity as a nonequilibrium steady state; we leave the search for this novel quantum phase to future work.

Another interesting direction for future research is the further study of amplitude equations in BECs. By their complex-valued nature, they are of a new type not seen in

other instances of pattern formation, and it will be crucial to understand their properties in applications to two-dimensional dipolar or spinor BECs [59–61]. Furthermore, BECs have been established as field simulators, e.g., in gravity analogs, and the amplitude equation could provide significant insight into instabilities and their stabilization mechanisms beyond the realm of pattern formation.

Acknowledgments. The authors thank T. Simula and F. Ziebert for stimulating discussions. This work was supported by Deutsche Forschungsgemeinschaft (German Research Foundation) under Project No. 273811115 (SFB1225 ISOQUANT) and under Germany’s Excellence Strategy EXC2181/1-390900948 (the Heidelberg STRUCTURES Excellence Cluster). This project was funded within the QuantERA II Programme that has received funding from the European Union’s Horizon 2020 research and innovation program under Grant Agreement No. 101017733. N.L. acknowledges support from the Studienstiftung des Deutschen Volkes.

-
- [1] M. C. Cross and P. C. Hohenberg, Pattern formation outside of equilibrium, *Rev. Mod. Phys.* **65**, 851 (1993).
- [2] M. C. Cross and H. Greenside, *Pattern Formation and Dynamics in Nonequilibrium Systems* (Cambridge University Press, Cambridge, 2009).
- [3] A. M. Turing, The chemical basis of morphogenesis, *Philos. Trans. R. Soc. London B* **237**, 37 (1952).
- [4] A. J. Koch and H. Meinhardt, Biological pattern formation: From basic mechanisms to complex structures, *Rev. Mod. Phys.* **66**, 1481 (1994).
- [5] K. Staliunas, S. Longhi, and G. J. de Valcárcel, Faraday patterns in Bose-Einstein condensates, *Phys. Rev. Lett.* **89**, 210406 (2002).
- [6] M. Faraday, XVII. On a peculiar class of acoustical figures; and on certain forms assumed by groups of particles upon vibrating elastic surfaces, *Philos. Trans. R. Soc. London* **121**, 299 (1831).
- [7] S. T. Milner, Square patterns and secondary instabilities in driven capillary waves, *J. Fluid Mech.* **225**, 81 (1991).
- [8] W. Zhang and J. Viñals, Square patterns and quasipatterns in weakly damped Faraday waves, *Phys. Rev. E* **53**, R4283 (1996).
- [9] C. Wagner, H. W. Müller, and K. Knorr, Crossover from a square to a hexagonal pattern in Faraday surface waves, *Phys. Rev. E* **62**, R33 (2000).
- [10] T. Simula, Droplet time crystals, *Phys. Scr.* **98**, 035004 (2023).
- [11] P. Engels, C. Atherton, and M. A. Hoefer, Observation of Faraday waves in a Bose-Einstein condensate, *Phys. Rev. Lett.* **98**, 095301 (2007).
- [12] J. H. V. Nguyen, M. C. Tsatsos, D. Luo, A. U. J. Lode, G. D. Telles, V. S. Bagnato, and R. G. Hulet, Parametric excitation of a Bose-Einstein condensate: From Faraday waves to granulation, *Phys. Rev. X* **9**, 011052 (2019).
- [13] D. Hernández-Rajkov, J. E. Padilla-Castillo, A. del Río-Lima, A. Gutiérrez-Valdés, F. J. Poveda-Cuevas, and J. A. Seman, Faraday waves in strongly interacting superfluids, *New J. Phys.* **23**, 103038 (2021).
- [14] K. Kwon, K. Mukherjee, S. J. Huh, K. Kim, S. I. Mistakidis, D. K. Maity, P. G. Kevrekidis, S. Majumder, P. Schmelcher, and J.-y. Choi, Spontaneous formation of star-shaped surface patterns in a driven Bose-Einstein condensate, *Phys. Rev. Lett.* **127**, 113001 (2021).
- [15] Z. Zhang, K.-X. Yao, L. Feng, J. Hu, and C. Chin, Pattern formation in a driven Bose-Einstein condensate, *Nat. Phys.* **16**, 652 (2020).
- [16] K. Staliunas, S. Longhi, and G. J. de Valcárcel, Faraday patterns in low-dimensional Bose-Einstein condensates, *Phys. Rev. A* **70**, 011601(R) (2004).
- [17] P. G. Kevrekidis and D. J. Frantzeskakis, Pattern forming dynamical instabilities of Bose-Einstein condensates, *Mod. Phys. Lett. B* **18**, 173 (2004).
- [18] A. I. Nicolin, R. Carretero-González, and P. G. Kevrekidis, Faraday waves in Bose-Einstein condensates, *Phys. Rev. A* **76**, 063609 (2007).
- [19] A. B. Bhattacharjee, Faraday instability in a two-component Bose-Einstein condensate, *Phys. Scr.* **78**, 045009 (2008).
- [20] P. Capuzzi and P. Vignolo, Faraday waves in elongated superfluid fermionic clouds, *Phys. Rev. A* **78**, 043613 (2008).
- [21] A. I. Nicolin and M. C. Raportaru, Faraday waves in high-density cigar-shaped Bose-Einstein condensates, *Physica A* **389**, 4663 (2010).
- [22] P. Capuzzi, M. Gattobigio, and P. Vignolo, Suppression of Faraday waves in a Bose-Einstein condensate in the presence of an optical lattice, *Phys. Rev. A* **83**, 013603 (2011).
- [23] R.-A. Tang, H.-C. Li, and J.-K. Xue, Faraday instability and Faraday patterns in a superfluid Fermi gas, *J. Phys. B: At. Mol. Opt. Phys.* **44**, 115303 (2011).
- [24] A. I. Nicolin, Resonant wave formation in Bose-Einstein condensates, *Phys. Rev. E* **84**, 056202 (2011).
- [25] J. Sabbatini, W. H. Zurek, and M. J. Davis, Phase separation and pattern formation in a binary Bose-Einstein condensate, *Phys. Rev. Lett.* **107**, 230402 (2011).
- [26] A. Balaž and A. I. Nicolin, Faraday waves in binary non-miscible Bose-Einstein condensates, *Phys. Rev. A* **85**, 023613 (2012).
- [27] A. I. Nicolin, Variational treatment of Faraday waves in inhomogeneous Bose-Einstein condensates, *Physica A* **391**, 1062 (2012).

- [28] K. Łakomy, R. Nath, and L. Santos, Faraday patterns in coupled one-dimensional dipolar condensates, *Phys. Rev. A* **86**, 023620 (2012).
- [29] F. K. Abdullaev, M. Ögren, and M. P. Sørensen, Faraday waves in quasi-one-dimensional superfluid Fermi-Bose mixtures, *Phys. Rev. A* **87**, 023616 (2013).
- [30] A. Balaž, R. Paun, A. I. Nicolin, S. Balasubramanian, and R. Ramaswamy, Faraday waves in collisionally inhomogeneous Bose-Einstein condensates, *Phys. Rev. A* **89**, 023609 (2014).
- [31] W. Cairncross and A. Pelster, Parametric resonance in Bose-Einstein condensates with periodic modulation of attractive interaction, *Eur. Phys. J. D* **68**, 106 (2014).
- [32] F. K. Abdullaev, A. Gammal, and L. Tomio, Faraday waves in Bose-Einstein condensates with engineering three-body interactions, *J. Phys. B: At. Mol. Opt. Phys.* **49**, 025302 (2016).
- [33] M. Conforti, A. Mussot, A. Kudlinski, S. Rota Nodari, G. Dujardin, S. De Bièvre, A. Armaroli, and S. Trillo, Heteroclinic structure of parametric resonance in the nonlinear Schrödinger equation, *Phys. Rev. Lett.* **117**, 013901 (2016).
- [34] J. B. Sudharsan, R. Radha, M. C. Raportaru, A. I. Nicolin, and A. Balaž, Faraday and resonant waves in binary collisionally-inhomogeneous Bose-Einstein condensates, *J. Phys. B: At. Mol. Opt. Phys.* **49**, 165303 (2016).
- [35] L. Tomio, A. Gammal, and F. K. Abdullaev, Faraday waves in cold-atom systems with two- and three-body interactions, *Few-Body Syst.* **58**, 52 (2017).
- [36] C.-X. Zhu, W. Yi, G.-C. Guo, and Z.-W. Zhou, Parametric resonance of a Bose-Einstein condensate in a ring trap with periodically driven interactions, *Phys. Rev. A* **99**, 023619 (2019).
- [37] D. Vudragović and A. Balaž, Faraday and resonant waves in dipolar cigar-shaped Bose-Einstein condensates, *Symmetry* **11**, 1090 (2019).
- [38] F. K. Abdullaev, A. Gammal, R. K. Kumar, and L. Tomio, Faraday waves and droplets in quasi-one-dimensional Bose gas mixtures, *J. Phys. B: At. Mol. Opt. Phys.* **52**, 195301 (2019).
- [39] B. K. Turmanov, B. B. Baizakov, and F. K. Abdullaev, Generation of density waves in dipolar quantum gases by time-periodic modulation of atomic interactions, *Phys. Rev. A* **101**, 053616 (2020).
- [40] D. K. Maity, K. Mukherjee, S. I. Mistakidis, S. Das, P. G. Kevrekidis, S. Majumder, and P. Schmelcher, Parametrically excited star-shaped patterns at the interface of binary Bose-Einstein condensates, *Phys. Rev. A* **102**, 033320 (2020).
- [41] K. Okazaki, J. Han, and M. Tsubota, Faraday waves in Bose-Einstein condensate: From instability to nonlinear dynamics, [arXiv:2012.02391](https://arxiv.org/abs/2012.02391).
- [42] G. Bougas, S. I. Mistakidis, and P. Schmelcher, Pattern formation of correlated impurities subjected to an impurity-medium interaction pulse, *Phys. Rev. A* **103**, 023313 (2021).
- [43] P. Oslaadisa, C. B. Tabi, and T. C. Kofané, Modulation instability in helicoidal spin-orbit coupled open Bose-Einstein condensates, *Phys. Rev. E* **103**, 052206 (2021).
- [44] Y. Cheng and Z.-Y. Shi, Many-body dynamics with time-dependent interaction, *Phys. Rev. A* **104**, 023307 (2021).
- [45] P. Díaz, L. Pérez, L. Reyes, D. Laroze, and J. Bragard, Taming Faraday waves in binary fermionic clouds: The effect of Zeeman interaction, *Chaos Soliton. Fract.* **153**, 111416 (2021).
- [46] H. Zhang, S. Liu, and Y.-S. Zhang, Faraday patterns in spin-orbit-coupled Bose-Einstein condensates, *Phys. Rev. A* **105**, 063319 (2022).
- [47] N. Shukuno, Y. Sano, and M. Tsubota, Faraday waves in Bose-Einstein condensates—The excitation by the modulation of the interaction and the potential, *J. Phys. Soc. Jpn.* **92**, 064602 (2023).
- [48] N. Liebster, M. Sparn, E. Kath, K. Fujii, S. L. Görlitz, T. Enss, H. Strobel, and M. K. Oberthaler, Emergence of crystalline steady state in a driven superfluid, [arXiv:2309.03792](https://arxiv.org/abs/2309.03792).
- [49] C. J. Pethick and H. Smith, *Bose-Einstein Condensation in Dilute Gases*, 2nd ed. (Cambridge University Press, Cambridge, 2008).
- [50] L. D. Landau and E. M. Lifshitz, *Mechanics* (Butterworth-Heinemann, Oxford, 1976), Vol. 1.
- [51] As discussed in the first paragraph of the Discussion, there is no relevant scattering between three modes satisfying $\mathbf{k}_1 + \mathbf{k}_2 + \mathbf{k}_3 = \mathbf{0}$ in our system due to the constraints imposed by the rotating-wave approximation, and scattering between four modes with $(\mathbf{k}, -\mathbf{k}, \mathbf{k}, -\mathbf{k})$ and $(\mathbf{k}, -\mathbf{k}, \mathbf{p}, -\mathbf{p})$ is dominant. For this reason, the ansatz with two distinct modes, as in Eq. (2), is sufficient.
- [52] See Supplemental Material at <http://link.aps.org/supplemental/10.1103/PhysRevA.109.L051301> for the derivation of the amplitude equation from the GP equation and the stability of the lattice pattern against fluctuations in the grid angle.
- [53] Since we have introduced the wave vectors \mathbf{k} and \mathbf{p} via the cosines in Eq. (2), the signs of them are irrelevant. Thus, we can take the angle θ being in $[0, \pi/2]$, and the case with $\theta \in [\pi/2, \pi]$ is given by replacing $\theta \in [0, \pi/2]$ with $\pi - \theta$.
- [54] As will be discussed below, the magnitude of Γ is irrelevant as long as the parameters allow for the occurrence of the Faraday instability at $\alpha > \Gamma$.
- [55] Figure 1 shows the direction of the second derivative given by Eq. (10), which represents the force. Also, since $\rho_{\mathbf{k},\mathbf{p}}$ is equal to the absolute value of the amplitude $R_{\mathbf{k},\mathbf{p}}$ on the plane with fixed $\nu_{\mathbf{k}} = \nu_{\mathbf{p}} = 0$, we simply denote $\rho_{\mathbf{k},\mathbf{p}}$ by $|R_{\mathbf{k},\mathbf{p}}|$.
- [56] L.-Y. Chen, N. Goldenfeld, and Y. Oono, Renormalization group theory for global asymptotic analysis, *Phys. Rev. Lett.* **73**, 1311 (1994).
- [57] T. Kunihiro, A geometrical formulation of the renormalization group method for global analysis, *Prog. Theor. Phys.* **94**, 503 (1995).
- [58] L.-Y. Chen, N. Goldenfeld, and Y. Oono, Renormalization group and singular perturbations: Multiple scales, boundary layers, and reductive perturbation theory, *Phys. Rev. E* **54**, 376 (1996).
- [59] R. Nath and L. Santos, Faraday patterns in two-dimensional dipolar Bose-Einstein condensates, *Phys. Rev. A* **81**, 033626 (2010).
- [60] T. Chen, K. Shibata, Y. Eto, T. Hirano, and H. Saito, Faraday patterns generated by Rabi oscillation in a binary Bose-Einstein condensate, *Phys. Rev. A* **100**, 063610 (2019).
- [61] S. M. Jose, K. Sah, and R. Nath, Patterns, spin-spin correlations and competing instabilities in driven quasi-two-dimensional spin-1 Bose-Einstein condensates, *Phys. Rev. A* **108**, 023308 (2023).